Dynamic Response of Syntactic Foams and Sandwich Composites: Blast and High Strain Rate Loading

Dung D. Luong, Luca Ansuini and Nikhil Gupta

1 Introduction

Foams are extensively used in weight sensitive applications. A variety of open and closed cell foams are used in marine systems. For example, closed-cell foam core sandwich structures are used in constructing ships and boats. One of the limitations of closed cell foams containing gas porosity is that the moisture can diffuse in the polymer and accumulate inside the gas pores, which can increase the effective density of the foam and result in degradation of the foam material over a long exposure period.

Some of these limitations are overcome by developing a special variety of closed cell foams, where thin-walled hollow particles are incorporated in a matrix material to create a foam-like microstructure. Existing applications of syntactic foams have been discussed in some of the available publications [1, 2]. Advantages of syntactic foams over conventional gas porosity foams include close control over the cell shape, size, and distribution. In addition, particle shell thickness and volume fraction can be controlled as two independent parameters in syntactic foams, which results in greater control over their properties. A combination of theoretical and experimental approaches has enabled methods of tailoring the properties of syntactic foams over a wide range, which is useful for the current and potential future applications of syntactic foams.

This chapter is focused on discussing the dynamic behavior of syntactic foam core materials under high strain rate compression and blast loading conditions. These loading conditions are relevant to their applications in lightweight armors and marine structures.

D. D. Luong · L. Ansuini · N. Gupta (✉)
Composite Materials and Mechanics Laboratory, Mechanical and Aerospace Engineering Department, New York University, Tandon School of Engineering, 6 MetroTech Center, Brooklyn, NY 11201, USA
e-mail: ngupta@nyu.edu
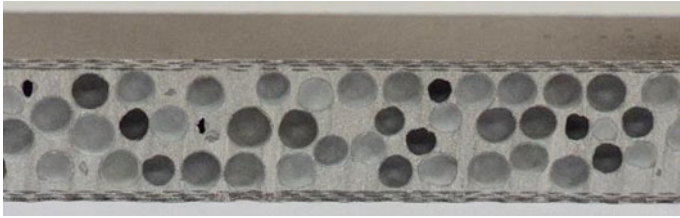
2   Syntactic Foams

A solid model representation of syntactic foam microstructure is shown in Fig. 1a, where hollow particles of various wall thicknesses can be observed dispersed in a matrix material. Figure 1b and c show examples of microstructures of polymer and metal matrix syntactic foams, respectively.

In both cases, hollow particles of different size scale are randomly dispersed in a matrix material. Polymer matrix syntactic foams have been extensively studied in the available literature to understand their mechanical, thermal, and electrical properties with respect to the parameters, such as matrix modulus, and particle modulus wall thickness and volume fraction. The lessons learned from polymer matrix syntactic foams are being extended to designing metal matrix syntactic foam microstructures.

In many applications, especially in structural applications that may be subjected to bending loads, syntactic foams are used in the form of sandwich structures. An example of a metal matrix syntactic foam core sandwich is shown in Fig. 2. In the present case, a carbon fabric is used as reinforcement in the skins. This sandwich is synthesized by one-step infiltration of the particle and fabric preform, so there is no interfacial layer between core and skins. Such sandwich structures are expected to have superior performance compared to the sandwich structures that contain skins adhesively bonded with the core.
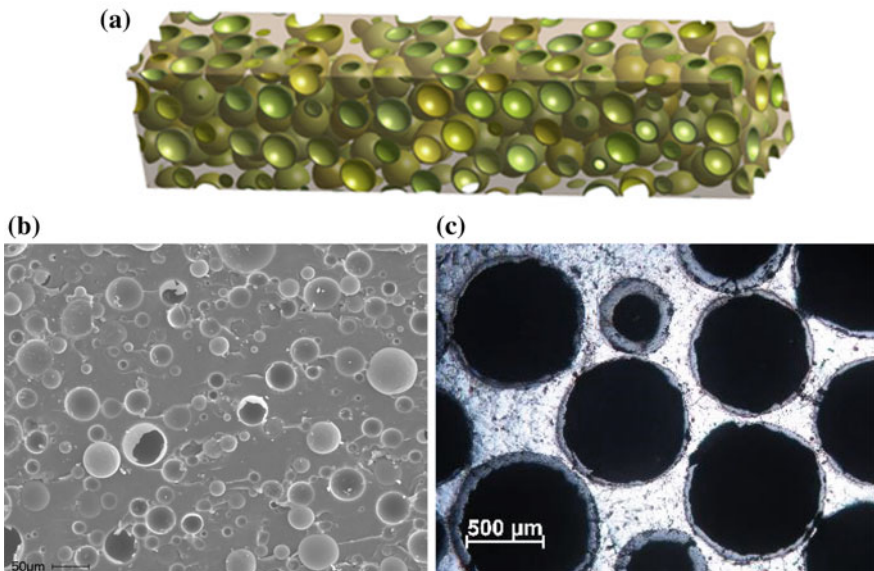
Fig. 1 **a** 3D model of syntactic foams filled hollow particles, **b** vinyl ester-glass microballoon syntactic foam, and **c** A356-SiC syntactic foam

Fig. 2 A metal matrix syntactic foam core sandwich containing carbon fabric skins
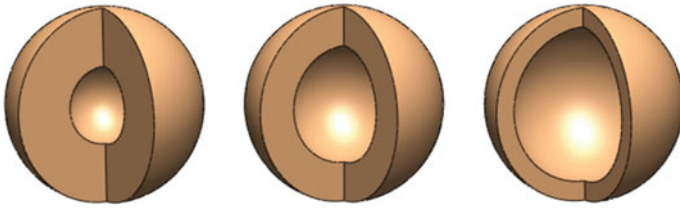

Fig. 3 Illustration of variation in wall thickness of particles of the same outer diameter. The true density of particles depends on the wall thickness

Although hollow particles of shapes such as cuboids, cylinders, and cones are available, only spherical particles have been used in synthesizing syntactic foams because spherical particles flow well in the mixture and provide isotropic properties to syntactic foams [3]. Figure 3 illustrates that particles of the same outer radius may have different wall thicknesses, which implies that the particle diameter, wall thickness, and volume fraction can be controlled independently in the syntactic foam.

Most of the available studies on polymer matrix syntactic foams have used glass particles of 1–300 μm diameter. The ratio of inner (r_i) to outer (r_o) radius of hollow particles is defined as radius ratio η. The available studies have mostly used particles of η greater than 0.85 to benefit from the low density of particles in that range. Increase in particle wall thickness increases the syntactic foam density, while a decrease in particle volume fraction increases the syntactic foam density. Studies are available that have focused on understanding the effects of these parameters on syntactic foam properties. An overview of properties of polymer and metal syntactic foams is presented in Fig. 4 and Fig. 5, respectively, where syntactic foams are grouped based on the matrix material. In most polymer syntactic foams glass microballoons (GMB) have been used as reinforcements. However, most studies on metal matrix syntactic foams have used SiC, Al_2O_3, or fly ash cenospheres as filler.

Figure 4 shows that polymer matrix syntactic foams are fabricated in the density range of 0.4–1.15 g/cm^3. It should be noted that particle wall thickness and volume fraction both can change the density of syntactic foams. In addition, fracture of particles during syntactic foam fabrication results in increased density, while entrapment of matrix porosity during mixing procedures results in a decreased

(a)

(b)
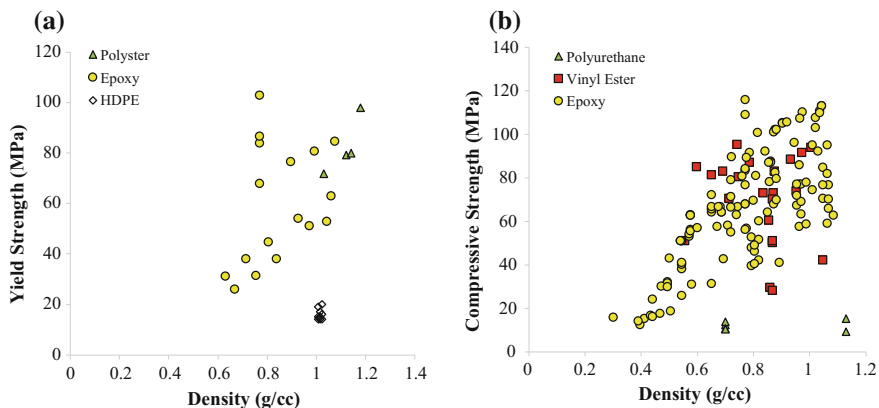
Fig. 4 a Yield strength (epoxy [4, 5], HDPE [6], polyester [7]), and **b** compressive strength (epoxy [4, 8–25], polyurethane [26, 27], vinyl ester [28–31]) of polymer matrix syntactic foams plotted against density

(a)

(b)
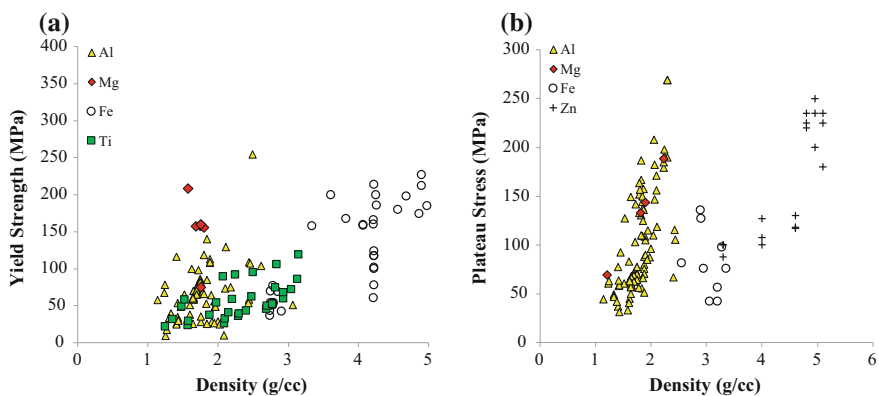
Fig. 5 a Yield strength (Al [32–42], Mg [43–45], iron [41, 46–55], Ti [56, 57]), **b** plateau stress (Al [34, 36, 38, 40, 42, 58–71], Mg [70, 72], iron [46, 71], Zn [73]) of metal syntactic foams plotted against density

density of the syntactic foam. The density in Fig. 4 includes the net effect of all these parameters on the density of the fabricated syntactic foams. In comparison, metal matrix syntactic foams have been fabricated in the density range of 1–5 g/cm³ as observed in Fig. 5. The properties of many compositions of syntactic foams are found to be superior compared to that of the matrix material, which is usually of higher density than the syntactic foams. Such observations show the possibility of weight saving in the structural application by using syntactic foams. A recent study showed a metal matrix syntactic foam with a density of 0.9 g/cm³ [74]. At such density levels, metal matrix syntactic foams start to compete with polymer matrix

syntactic foams in applications, where higher load bearing capacity or higher temperature withstanding capabilities are required.

The present chapter does not include discussion on particle-matrix interfacial bonding and particle to particle interactions. However, these effects have been studied by experimental and simulation methods [75–77].

3 High Strain Rate Properties of Syntactic Foams

The split-Hopkinson pressure bar (SHPB) setup has been widely used for high strain rate characterization of syntactic foams. This technique assumes one-dimensional wave propagation and neglects temperature rise and inertia effects in the specimens. Extensive literature is available on this technique that mostly reports on the strength parameters, not the modulus. Testing of syntactic foams using SHPB is especially challenging due to the high volume fraction of porosity in their structure, resulting in a weak transmitted signal. In addition, pulse shaping is very important in testing foams because it can provide enough time to obtain the stress equilibrium in the specimen during deformation.

Figure 6 shows the compressive strength of polymer matrix syntactic foams with respect to strain rate. The low strain rate results are obtained using universal test systems and the high strain rate results are obtained using the SHPB technique. The strength is found to increase with strain rate. In many cases, the high strain rate strength is found be to twice the quasi-static strength. These experimental measurements emphasize the need for using the correct properties of materials in designing armors and protective structures that are intended for use under high strain rate loading conditions.

Fig. 6 Compressive strength of polymer matrix SFs [4, 11, 19, 22, 26, 30, 81] plotted against strain rate
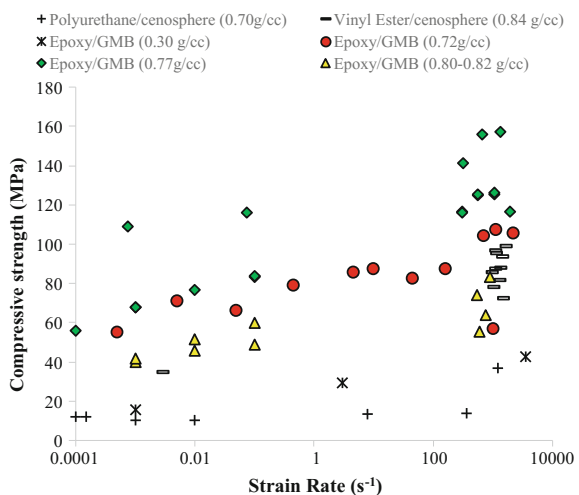
Among the main effects of high strain rate loading of polymer matrix syntactic foams are suppression of elastic deformation and increase in brittleness. The effect of an increase in strain rate on material behavior is similar to decrease in temperature and previous studies have converted the temperature dependent mechanical property data to strain rate dependent material response [78, 79]. Understanding such effects is crucial for fully characterizing the materials across the entire spectrum of temperatures and strain rates.

Observations of polymer matrix syntactic foam failure behavior are shown in Fig. 7. It is observed that the failure mechanism of syntactic foams changes from shear to brittle failure as the strain rate is increased. Brittle failure results in less hollow particle crushing and increased specimen fragmentation. However, these trends are dependent on the total porosity present in the syntactic foam microstructure [80]. Highly porous foams have shown softening with increasing strain rate while foams with less porosity have shown stiffening effect with increasing strain rate.

The high strain rate behavior of some metal matrix syntactic foams is summarized in Fig. 8. Iron and aluminum matrix syntactic foams are covered in this figure. The body-centered cubic structure of iron is found to be strain rate sensitive while the face-centered cubic structure of aluminum is found to be relatively insensitive to strain rate in the range tested by split-Hopkinson pressure bar. The strength of iron syntactic foams is almost doubled from quasi-static compression to about 5000 s^{-1} strain rate. This figure also shows that the strength of iron and aluminum syntactic foams is over 100 MPa for many compositions, which can help in developing their load bearing applications. The properties measured at various strain rates can be used as input for the finite element analysis studies to conduct parametric studies and understand the behavior of the material over a wide range of composition and loading parameters.

Fig. 7 Vinyl ester matrix syntactic foam containing 60 vol.% of 460 kg/m^3 GMB **a** tested at 920 s^{-1} strain rate, **b** CT scan showing shear cracks. The same material **c** tested at 1260 s^{-1} strain rate and **d** CT scan showing primarily brittle fracture
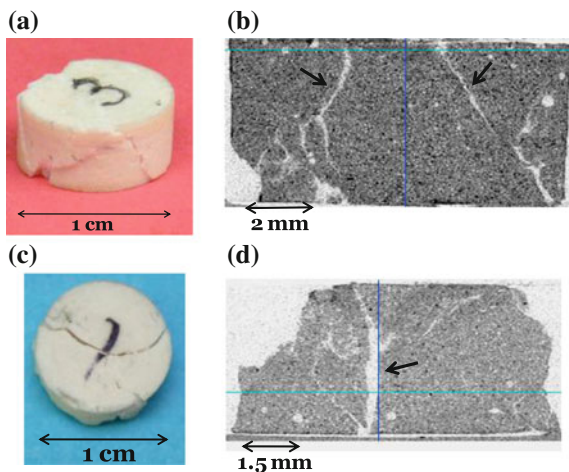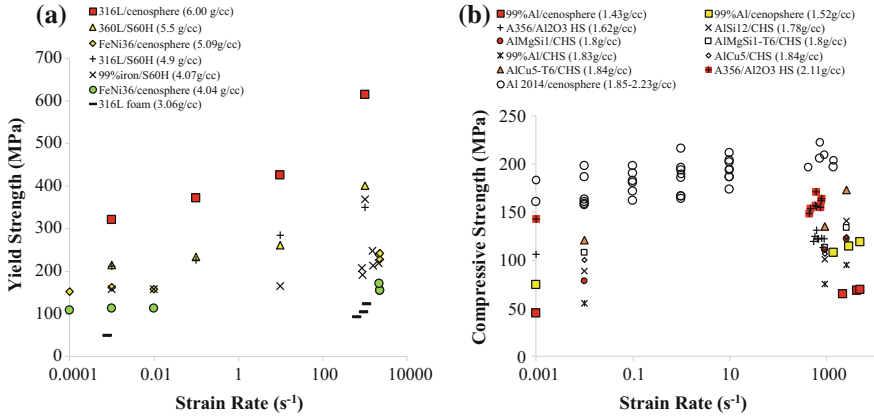
Fig. 8 **a** Yield strength of iron-based matrix SFs [41, 50, 52, 54, 55] and **b** compressive strength of aluminum SFs [39, 40, 60, 66, 82] plotted against strain rate
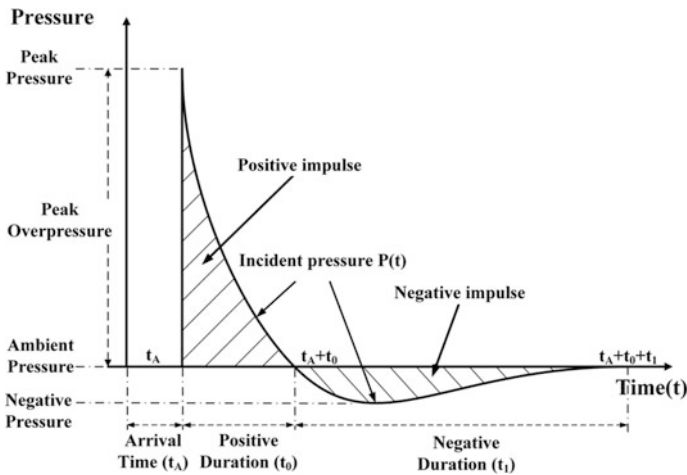
Fig. 9 A typical blast wave profile. Adapted from [83]

4 Blast Properties of Syntactic Foams

4.1 Shock Wave

A typical blast wave profile with respect to time is plotted in Fig. 9 [83]. The blast wave forms by a sudden release of energy, such as an explosion, and consists of a shock front in which pressure rises instantaneously from the ambient pressure (P_a) to a high value of P_s. The pressure decays exponentially with time. This is followed

by a negative pressure phase in which the air expands to return the pressure to the ambient value. The development and propagation of blast wave are expressed by the Friedlander equation [84, 85]

$$P(t) = (P_s - P_a)\left[1 - \frac{t - t_A}{t_0}\right]e^{-(t - t_A)/\theta} + P_a \qquad (1)$$

where t_A is the arrival time of the blast wave, t_0 is the duration of the positive phase in which the pressure rises to the peak and then returns to the ambient value, and θ is a decay-time constant. The damage potential of a blast wave depends on its positive phase and the impulse loading, I, specified by

$$I = \int_0^{t_0} P(t)dt \qquad (2)$$

The implications of expansion wave are significant on syntactic foams because of their low mechanical properties under tensile loading conditions. Particle-matrix debonding and matrix cracking may occur, especially for brittle resin systems during the tensile loading phase. Nonetheless, the standoff distance is one of the most important parameters in blast wave–structure interactions.

4.2 Shock Wave Propagation in Syntactic Foams

Finite element analysis (FEA) simulations are conducted to understand the shock wave-syntactic foam interactions and the material deformation and failure mechanisms. The simulations are conducted using Ansys AUTODYN commercial software (v.18.0). The results obtained from high strain rate testing of the matrix resin and syntactic foams are used as input parameters for these simulations to have a more realistic material behavior at the applied strain rates. The objective is to observe and predict the one-dimensional shock wave propagation in syntactic foams of pure iron matrix filled with 45 vol.% of 3M[TM] S60HS soda lime GMBs as reported in [50, 54, 86]. Figure 10 depicts a $300 \times 150~\mu m^2$ 2D domain

**Fig. 10** The model of 1D blast propagation in syntactic foam
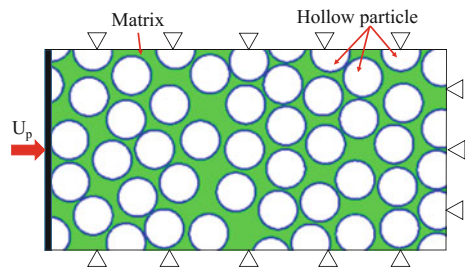
representing the microstructure of pure iron syntactic foams containing GMBs of 30 μm diameter and 1.3 μm wall thickness [50, 87]. The domain contains 49 particles, some of which are partially inside the domain. The GMBs are randomly dispersed in the matrix by using an in-house MATLAB code. In order to simulate the behavior of syntactic foams under shock wave, the Euler mesh is used to discretize the domain and the mesh size is set to 0.65 μm to make sure that the GMB walls contain at least two elements. Smaller mesh sizes took significantly longer time to converge.

The idealized 1D shock compression is generated by applying a particle velocity U_p to the left side of the model and roller support to other sides, as shown in Fig. 10 [88]. In Eulerian finite element model, the stress–strain constitutive model of the materials is separated and distinguished in the hydrostatic and deviatoric components. The hydrostatic component is represented by the equation of state (EOS). Both pure iron and soda lime glass materials use the Hugoniot linear EOS reposted in [89, 90], respectively. Besides the deviatoric component is calculated by the strength model. Hence, the Johnson-Cook strength model of pure iron [91] is applied.

Figure 11 shows the deformation microstructure of iron syntactic foams at four different time steps when the material is deformed with 1 km/s rate. The collapsed GMBs consolidate in the cavity and the material densifies as the shock wave
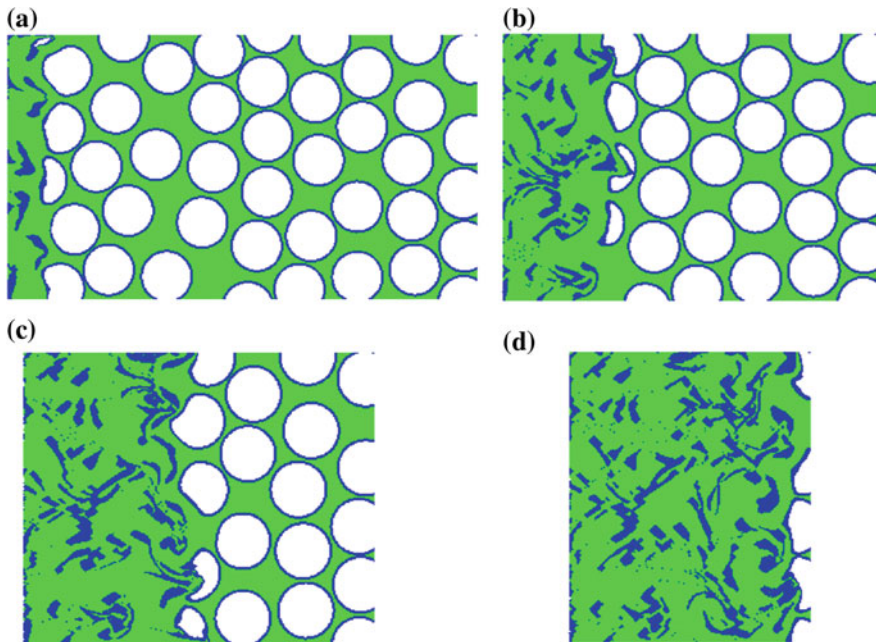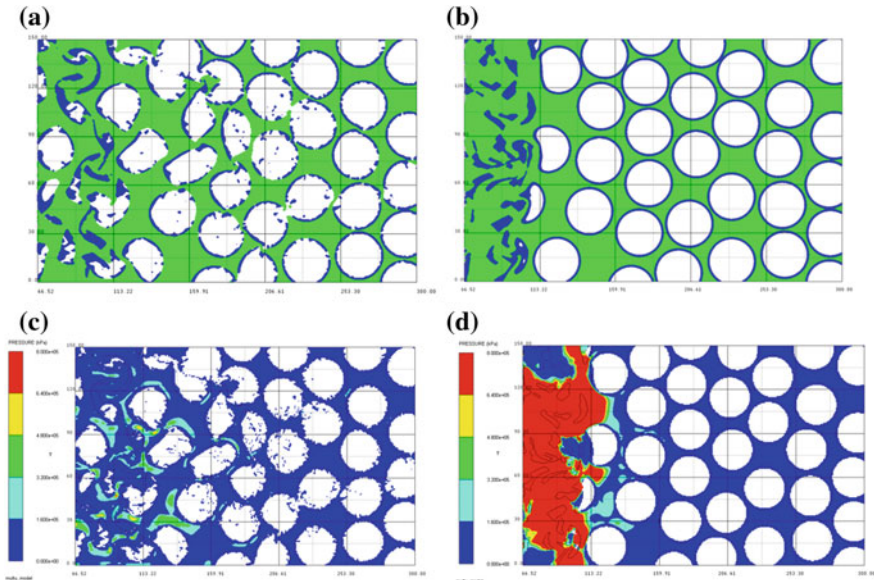

Fig. 11 The deformation microstructures of iron syntactic foams at time of **a** $t = 0.028$ μs **b** 0.085 μs **c** 0.113 μs **d** 0.170 μs for $U_p = 1$ km/s

propagates. The elastic nature of iron results in large deformation of the matrix being required for densification in the GMB cavity.

Results for incident shock velocities of 0.1 and 0.8 km/s are compared in Fig. 12, where the deformed microstructure and pressure distribution inside the microstructure are represented. At faster shock velocities, the microstructure completely densifies as the shock front propagates. In comparison, the densification front lags behind the shock front at slower shock velocities. The microstructure also shows that the material compression results in fracture of particles in the entire specimen at slow shock speed, whereas the particles are intact away from the shock interaction zone in the specimen subjected to faster shock velocity.

Figure 12c and d show that the pressure is distributed more uniformly in the microstructure at slower shock velocities, whereas the pressure concentration is observed close to the incident wave side of the microstructure at higher shock velocity. Uniform distribution of pressure in the entire microstructure results in particle fracture throughout the specimen.

In this study, the shock wave velocity (U_S) is determined by averaging the horizontal velocity at 12 measurement points that are located at the same horizontal location and along the vertical direction at the beginning and move following the deformation of the material in the domain. The U_S is found to be slightly higher than U_P, which is likely because the shock wave propagation in the syntactic foam is similar to the densification process of the cellular material.



Fig. 12 The **a**, **b** deformed microstructures and **c**, **d** pressure distribution of iron syntactic foams having the same deformation of 66.52 μm for **a**, **c** U_p = 0.1 km/s and **b**, **d** 0.8 km/s

The results presented in Figs. 11 and 12 show the response of only a limited set of syntactic foams and loading conditions. However, syntactic foams can be tailored for a wide range of behaviors under shock loading by changing the particle wall thickness and volume fraction. One of the limitations of this approach can be that a given composition of syntactic foams may be most effective for energy absorption under a narrow range of shock properties. Functionally graded syntactic foams with a gradient in the wall thickness or volume fraction along the material thickness may be effective in mitigating the effects of a wide range of shock types [92, 93].

4.3 Blast Mitigation of Sandwich Composite

The dynamic response of a syntactic foam core sandwich composite panel under blast wave is simulated in ABAQUS. Syntactic foam core sandwich panels have been fabricated with a wide range of materials, including polymers and metals [94–96], and have been studied for various properties. In addition to the tailoring of the syntactic foams core by means of material selection and selection of particle properties, additional tailoring parameters are available in sandwich structures in the form of skin fabric, lay up sequence, and thickness of the skins. Optimization of all these parameters is a challenging task and can only be conducted based on a given threat level. Some of the fundamental aspects of modeling the sandwich behavior are presented below.

The quarter symmetry model is built as a rectangular panel of dimensions 100×75 mm^2 with a thickness of 20 mm for the syntactic foam core and 0.4 mm for the fiber reinforced laminate skins. The skins contain two layers of fabric in 0/90 orientation as shown in Fig. 13a. Figure 13b shows the symmetry boundary conditions applied to two edges and clamped supports applied to two other edges.
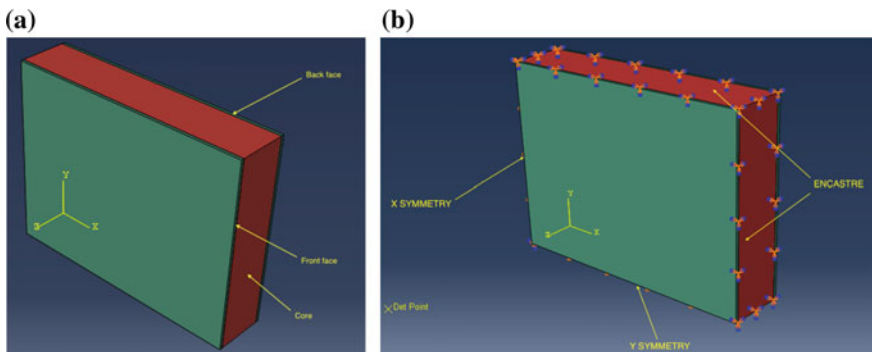
Fig. 13 a A representative syntactic foam core sandwich panel model used in simulations and **b** the applied boundary conditions

The blast load is created by a 50 g TNT explosion with the standoff distance of 90 mm by the CONWEP feature [97].

The syntactic foam core comprises vinyl ester (VE) matrix filled with glass microballoons. The properties of four types of core materials simulated in this study are presented in Table 1. These properties are obtained from an experimental study [28]. The constitutive model of core material includes a linear elastic model followed by a crushable foam model in the plasticity range [97] that was developed from the isotropic foam constitutive model published by Deshpande and Fleck [98]. The crushable foam parameters are estimated from the literature [28, 31] and are listed in Table 2.

The fiber reinforced laminated skin is modeled as a brittle material with orthotropic elastic behavior. Its Young's moduli (E), Poisson's ratios (ν), and shear moduli (G) are listed in Table 3. The failure criteria of the laminate is set up with Hashin damage model that contains four different modes of failure: fiber rupture in tension, fiber buckling and wrinkling in compression, matrix cracking under transverse tension and shearing, and matrix crushing under transverse compression and shearing. The parameters of the Hashin damage model include longitudinal tensile ($X^T = 270$ MPa), longitudinal compressive ($X^C = 200$ MPa), transverse tensile ($Y^T = 270$ MPa), transverse compressive ($Y^C = 200$ MPa), longitudinal shear ($S^L = 40$ MPa), and transverse shear ($S^T = 31.6$ MPa) strengths.

The von-Mises stress distribution on the face sheets is shown in Fig. 14a for VE-220-30 syntactic foam core sandwich. Part of the syntactic foam core reaches plastic condition as shown in Fig. 14b. As expected it happens in the proximity of the front face sheet, while the back face stress is lower. The plastic strain is maximum at the center of the front face and gradually reduces in magnitude toward the clamped edges. The sandwich panel reaches the maximum deflection in about 0.1 ms when the interaction with the blast wave takes place. After that, the core absorbed part of the kinetic energy coming from the blast by plastic deformation. When plastic deformation ended, the elastic response of the sandwich panel causes continuous oscillations that decay over time.

The front and back skin deflections of different VE syntactic foam core panels are plotted over time in Fig. 15. The equilibrium deflection values for syntactic foams are listed in Table 4. These values represent plastic strain in the material.

Tailoring the particle type and volume fraction affects the stiffness of the syntactic foam and helps in managing the deflection. In addition, as observed in the

Table 1 The mechanical VE syntactic foams

Material	Volume fraction (%)	Density (kg/m^3)	Peak stress (MPa)	E (GPa)	Plateau stress (MPa)
VE220-30	30	870	66.11	1.66	64.46
VE220-60	60	558	33.08	0.80	31.50
VE460-30	30	930	100.64	1.27	89.65
VE460-60	60	734	84.11	1.15	74.42

Table 2 The crushable foam parameters of polymer syntactic foam core materials.[a]

Material	k	k_t	R	$\dot{\overline{\varepsilon^{pl}}}$	Material	k	k_t	R	$\dot{\overline{\varepsilon^{pl}}}$
VE220-30	1.08	0.1	1	0.0001	VE460-30	1.5	0.1	1	0.0001
			1.158	0.001				1.103	0.001
			1.223	0.01				1.097	0.01
			1.172	0.1				1.178	0.1
			1.8	1024				1.565	793
			1.936	1155				1.609	1008
			1.785	1215				1.563	1127
			1.906	1457				1.559	1172
			1.694	1547				1.465	1401
								1.610	1535
								1.552	1796
VE220-60	1.2	0.1	1	0.0001	VE460-60	1.08	0.1	1	0.0001
			1.095	0.001				1.119	0.001
			1.146	0.01				1.151	0.01
			1.157	0.1				1.142	0.1
			1.663	1276				1.275	818
			1.451	1342				1.328	997
			1.632	1474				1.357	1236
			1.693	1579				1.386	1269
			1.602	1814				1.398	1286
			1.693	2121				1.378	1667
			1.511	2687				1.335	1851

[a]Notations: $k = \sigma_c^o / p_c^o$ is defined as the compressive yield strength ratio; $k_t = p_t^o / p_c^o$ is hydrostatic yield stress ratio; $R = \overline{\sigma}_c / \sigma_c$ is yield stress ratio; and $\dot{\overline{\varepsilon^{pl}}}$ is equivalent plastic strain rate. σ_c^o is the initial compressive yield stress; p_c^o and p_t^o are respectively the initial compressive yield stress under hydrostatic load and the initial tensile yield stress under hydrostatic load. R is given as the set of data corresponding to equivalent plastic strain rate $\dot{\overline{\varepsilon^{pl}}}$

Table 3 Orthotropic elastic properties of the fiber reinforced sheet

E_1 GPa	E_2 GPa	E_3 GPa	ν_{12}	ν_{13}	ν_{23}	G_{12} GPa	G_{13} GPa	G_{23} GPa
17	17	7.48	0.13	0.28	0.13	4	1.730	1.730

case of microstructure-based simulations of iron syntactic foams, the particle crushing behavior can be controlled by selecting particles of appropriate wall thickness. Such possibilities can provide the energy absorption capabilities as per the material design and develop syntactic foam core and sandwich structure as per the anticipated loading conditions.
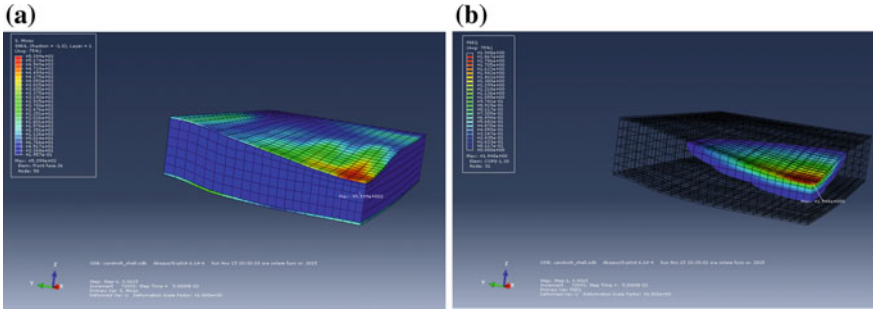
Fig. 14 a The distribution of von-Misses stress of VE220-30 and **b** equivalent plastic strain inside VE220-30 core plotted as isosurface contour
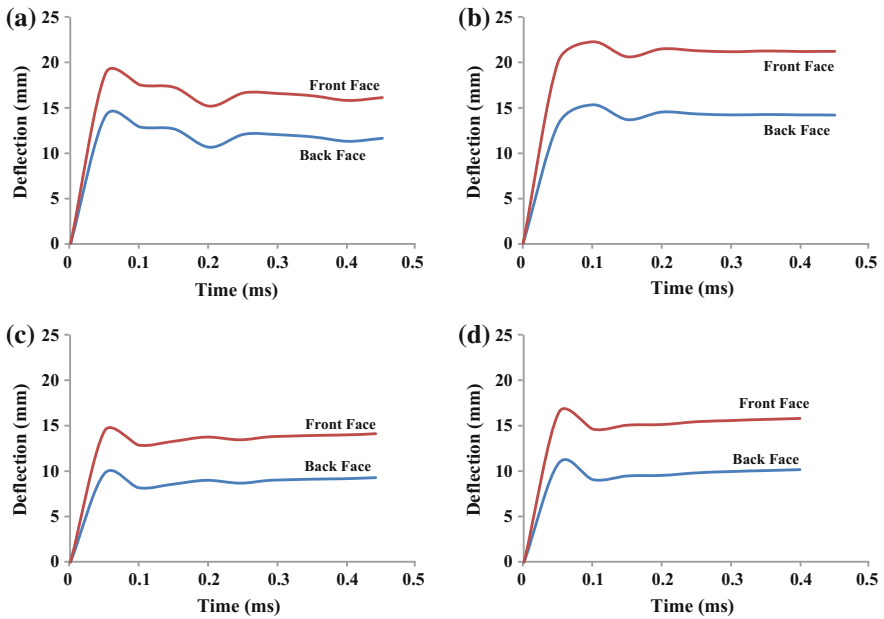
Fig. 15 Front and back sheet deflections of **a** VE220-30, **b** VE220-60, **c** VE460-30, and **d** VE460-60 core panel plotted against time

Table 4 Defection of front and back laminate sheets at equilibrium

Core material	Deflection of back face (mm)	Deflection of front face (mm)	Relative deflection (mm)
VE220-30	14.20	18.80	4.60
VE220-60	13.21	20.05	6.84
VE460-30	9.89	14.54	4.65
VE460-60	10.91	16.52	5.61

The effects of temperature on the blast loading response of structures can be significant, but have not been studied in detail so far. For example, the same panel loaded under arctic temperature conditions versus desert temperature conditions can produce very different results due to brittleness effects. Such parameters should be combined with the loading and microstructure-based parameters to fully characterize the material for a given scenario.

5 Conclusions

Thin-walled particles and porosity present in syntactic foam microstructure result in a difference in failure mechanisms as the loading condition is changed from quasi-static to high strain rate. Studies have shown that the failure mechanism of syntactic foams can change from shear to brittle fracture as the loading condition is changed from quasi-static to high strain rate. The strain rate sensitivity is also observed in the measured mechanical properties of syntactic foams. Studies are available on blast loading of syntactic foams and their sandwich structures. These materials need to be tailored as per a given threat level because of the number of parameters available to tailor their properties. For example, a number of combinations of particle wall thickness and volume fractions can provide the same density or mechanical properties which facilitate the selection of the most optimal material for the given loading condition.

References

1. Gupta, N., Zeltmann, S. E., Shunmugasamy, V. C., & Pinisetty, D. (2014). Applications of polymer matrix syntactic foams. *JOM, 66*(2), 245–254.
2. Gupta, N., Pinisetty, D., & Shunmugasamy, V. C. (2013). *Reinforced polymer matrix syntactic foams: Effect of nano and micro-scale reinforcement*. SpringerBriefs in Materials. Springer.
3. Gupta, N., & Rohatgi, P. K. (Eds.). (2014). *Metal matrix syntactic foams: Processing, microstructure, properties and applications*. DEStech Publications: Lancaster, PA.
4. Song, B., Chen, W., Yanagita, T., & Frew, D. J. (2005). Confinement effects on the dynamic compressive properties of an epoxy syntactic foam. *Composite Structures, 67*(3), 279–287.
5. Huang, C., Huang, Z., Qin, Y., Ding, J., & Lv, X. (2016). Mechanical and dynamic mechanical properties of epoxy syntactic foams reinforced by short carbon fiber. *Polymer Composites, 37*(7), 1960–1970.
6. Bharath Kumar, B. R., Singh, A. K., Doddamani, M., Luong, D. D., & Gupta, N. (2016). Quasi-static and high strain rate compressive response of injection-molded cenosphere/HDPE syntactic foam. *JOM, 68*(7), 1861–1871.

 7. Rohatgi, P. K., Matsunaga, T., & Gupta, N. (2009). Compressive and ultrasonic properties of polyester/fly ash composites. *Journal of Materials Science, 44*(6), 1485.
 8. Gupta, N., Woldesenbet, E., & Mensah, P. (2004). Compression properties of syntactic foams: effect of cenosphere radius ratio and specimen aspect ratio. *Composites Part A: Applied Science and Manufacturing, 35*(1), 103–111.
 9. Woldesenbet, E., & Peter, S. (2009). Volume fraction effect on high strain rate properties of syntactic foam composites. *Journal of Materials Science, 44*(6), 1528–1539.
10. Woldesenbet, E., & Peter, S. (2008). Radius ratio effect on high-strain rate properties of syntactic foam composites. *Journal of Materials Science, 44*(6), 1551.
11. Li, P., Petrinic, N., Siviour, C. R., Froud, R., & Reed, J. M. (2009). Strain rate dependent compressive properties of glass microballoon epoxy syntactic foams. *Materials Science and Engineering: A, 515*(1–2), 19–25.
12. Xie, W., Yan, H., Mei, Q., Du, M., & Huang, Z. (2007). Compressive and fracture properties of syntactic foam filled with hollow plastic bead (HPC). *Journal of Wuhan University of Technology-Materials Science Edition, 22*(3), 499–501.
13. Ambika Devi, K., John, B., Reghunadhan Nair, C. P., & Ninan, K. N. (2007). Syntactic foam composites of epoxy-allyl phenol-bismaleimide ternary blend—Processing and properties. *Journal of Applied Polymer Science, 105*(6), 3715–3722.
14. Kishore, Shankar, R., & Sankaran, S. (2006). Effects of microballoons' size and content in epoxy on compressive strength and modulus. *Journal of Materials Science, 41*(22), 7459–7465
15. Wouterson, E. M., Boey, F. Y. C., Hu, X., & Wong, S.-C. (2005). Specific properties and fracture toughness of syntactic foam: Effect of foam microstructures. *Composites Science and Technology, 65*(11–12), 1840–1850.
16. Karthikeyan, C.S., Sankaran, S., Jagdish Kumar, M.N., & Kishore. (2001). Processing and compressive strengths of syntactic foams with and without fibrous reinforcements. *Journal of Applied Polymer Science, 81*(2), 405–411.
17. Dimchev, M., Caeti, R., & Gupta, N. (2010). Effect of carbon nanofibers on tensile and compressive characteristics of hollow particle filled composites. *Materials and Design, 31*(3), 1332–1337.
18. Gupta, N., & Maharsia, R. (2005). Enhancement of energy absorption in syntactic foams by nanoclay incorporation for sandwich core applications. *Applied Composite Materials, 12*(3), 247–261.
19. Song, B., Chen, W., & Frew, D. J. (2004). Dynamic compressive response and failure behavior of an epoxy syntactic foam. *Journal of Composite Materials, 38*(11), 915–936.
20. Viot, P., Shankar, K., & Bernard, D. (2008). Effect of strain rate and density on dynamic behaviour of syntactic foam. *Composite Structures, 86*(4), 314–327.
21. Peter, S., & Woldesenbet, E. (2008). Nanoclay syntactic foam composites—High strain rate properties. *Materials Science and Engineering: A, 494*(1–2), 179–187.
22. Song, B., Chen, W. W., & Lu, W. Y. (2007). Mechanical characterization at intermediate strain rates for rate effects on an epoxy syntactic foam. *International Journal of Mechanical Sciences, 49*(12), 1336–1343.
23. Drdlová, M., & Prachař, V. (2016). High strain rate characteristics of nanoparticle modified blast energy absorbing materials. *Procedia Engineering, 151,* 214–221.
24. Ahmadi, H., Liaghat, G. H., Shokrieh, M. M., Hadavinia, H., Ordys, A., & Aboutorabi, A. (2014). Quasi-static and dynamic compressive properties of ceramic microballoon filled syntactic foam. *Journal of Composite Materials, 49*(10), 1255–1266.
25. Ahmadi, H., Liaghat, G. H., Shokrieh, M. M., Aboutorabi, A., Hadavinia, H., & Ordys, A. (2014). Compressive properties of nanoclay-reinforced syntactic foams at quasi-static and high strain rate loading. *Polymer-Plastics Technology and Engineering, 53*(10), 990–999.
26. Pellegrino, A., Tagarielli, V. L., Gerlach, R., & Petrinic, N. (2015). The mechanical response of a syntactic polyurethane foam at low and high rates of strain. *International Journal of Impact Engineering, 75,* 214–221.

27. Luong, D. D., Shunmugasamy, V. C., Strbik III, O. M., & Gupta, N. (2014). High strain rate compressive behavior of polyurethane resin and polyurethane/Al_2O_3 hollow sphere syntactic foams. *Journal of Composites,* Article ID 795984.

28. Gupta, N., Ye, R., & Porfiri, M. (2010). Comparison of tensile and compressive characteristics of vinyl ester/glass microballoon syntactic foams. *Composites Part B: Engineering, 41*(3), 236–245.

29. Labella, M., Shunmugasamy, V. C., Strbik, O. M., & Gupta, N. (2014). Compressive and thermal characterization of syntactic foams containing hollow silicon carbide particles with porous shell. *Journal of Applied Polymer Science, 131*(17), 8593–8597.

30. Labella, M., Zeltmann, S. E., Shunmugasamy, V. C., Gupta, N., & Rohatgi, P. K. (2014). Mechanical and thermal properties of fly ash/vinyl ester syntactic foams. *Fuel, 121,* 240–249.

31. Shunmugasamy, V. C., Gupta, N., Nguyen, N. Q., & Coelho, P. G. (2010). Strain rate dependence of damage evolution in syntactic foams. *Materials Science and Engineering: A, 527*(23), 6166–6177.

32. Rohatgi, P. K., Kim, J. K., Gupta, N., Alaraj, S., & Daoud, A. (2006). Compressive characteristics of A356/fly ash cenosphere composites synthesized by pressure infiltration technique. *Composites Part A: Applied Science and Manufacturing, 37*(3), 430–437.

33. Sudarshan, & Surappa, M. K. (2008). Synthesis of fly ash particle reinforced A356 Al composites and their characterization. *Materials Science and Engineering: A, 480*(1–2), 117–124.

34. Tao, X. F., Zhang, L. P., & Zhao, Y. Y. (2009). Al matrix syntactic foam fabricated with bimodal ceramic microspheres. *Materials and Design, 30*(7), 2732–2736.

35. Luong, D. D., Gupta, N., Daoud, A., & Rohatgi, P. K. (2011). High strain rate compressive characterization of aluminum alloy/fly ash cenosphere composites. *JOM, 63*(2), 53–56.

36. Májlinger, K., & Orbulov, I. N. (2014). Characteristic compressive properties of hybrid metal matrix syntactic foams. *Materials Science and Engineering: A, 606,* 248–256.

37. Vogiatzis, C. A., Tsouknidas, A., Kountouras, D. T., & Skolianos, S. (2015). Aluminum–ceramic cenospheres syntactic foams produced by powder metallurgy route. *Materials and Design, 85,* 444–454.

38. Szlancsik, A., Katona, B., Májlinger, K., & Orbulov, I. (2015). Compressive behavior and microstructural characteristics of iron hollow sphere filled aluminum matrix syntactic foams. *Materials, 8*(11), 5432.

39. Myers, K., Katona, B., Cortes, P., & Orbulov, I. N. (2015). Quasi-static and high strain rate response of aluminum matrix syntactic foams under compression. *Composites Part A: Applied Science and Manufacturing, 79,* 82–91.

40. Licitra, L., Luong, D. D., Strbik III, O. M., & Gupta, N. (2015). Dynamic properties of alumina hollow particle filled aluminum alloy A356 matrix syntactic foams. *Materials and Design, 66, Part B*, 504–515.

41. Alvandi-Tabrizi, Y., Whisler, D. A., Kim, H., & Rabiei, A. (2015). High strain rate behavior of composite metal foams. *Materials Science and Engineering: A, 631,* 248–257.

42. Zhang, B., Lin, Y., Li, S., Zhai, D., & Wu, G. (2016). Quasi-static and high strain rates compressive behavior of aluminum matrix syntactic foams. *Composites Part B: Engineering, 98,* 288–296.

43. Daoud, A., Abou El-khair, M. T., Abdel-Aziz, M., & Rohatgi, P. (2007). Fabrication, microstructure and compressive behavior of ZC63 Mg-microballoon foam composites. *Composites Science and Technology, 67*(9), 1842–1853.

44. Rohatgi, P. K., Daoud, A., Schultz, B. F., & Puri, T. (2009). Microstructure and mechanical behavior of die casting AZ91D-Fly ash cenosphere composites. *Composites Part A: Applied Science and Manufacturing, 40*(6–7), 883–896.

45. Luong, D. D., Gupta, N., & Rohatgi, P. K. (2011). The high strain rate compressive response of Mg-Al alloy/fly Ash cenosphere composites. *JOM, 63*(2), 48–52.

46. Brown, J., Vendra, L., & Rabiei, A. (2010). Bending properties of Al-steel and steel-steel composite metal foams. *Metallurgical and Materials Transactions A, 41*(11), 2784–2793.

47. Weise, J., Baumeister, J., Yezerska, O., Salk, N., & Silva, G. B. D. (2010). Syntactic iron foams with integrated microglass bubbles produced by means of metal powder injection moulding. *Advanced Engineering Materials, 12*(7), 604–608.

48. Castro, G., & Nutt, S. R. (2012). Synthesis of syntactic steel foam using mechanical pressure infiltration. *Materials Science and Engineering: A, 535,* 274–280.

49. Castro, G., & Nutt, S. R. (2012). Synthesis of syntactic steel foam using gravity-fed infiltration. *Materials Science and Engineering: A, 553,* 89–95.

50. Peroni, L., Scapin, M., Avalle, M., Weise, J., & Lehmhus, D. (2012). Dynamic mechanical behavior of syntactic iron foams with glass microspheres. *Materials Science and Engineering: A, 552,* 364–375.

51. Rabiei, A., & Garcia-Avila, M. (2013). Effect of various parameters on properties of composite steel foams under variety of loading rates. *Materials Science and Engineering: A, 564,* 539–547.

52. Peroni, L., Scapin, M., Fichera, C., Lehmhus, D., Weise, J., Baumeister, J., et al. (2014). Investigation of the mechanical behaviour of AISI 316L stainless steel syntactic foams at different strain-rates. *Composites Part B: Engineering, 66,* 430–442.

53. Weise, J., Lehmhus, D., Baumeister, J., Kun, R., Bayoumi, M., & Busse, M. (2014). Production and properties of 316L stainless steel cellular materials and syntactic foams. *Steel Research International, 85*(3), 486–497.

54. Luong, D. D., Shunmugasamy, V. C., Gupta, N., Lehmhus, D., Weise, J., & Baumeister, J. (2015). Quasi-static and high strain rates compressive response of iron and Invar matrix syntactic foams. *Materials and Design, 66, Part B,* 516–531.

55. Luong, D., Lehmhus, D., Gupta, N., Weise, J., & Bayoumi, M. (2016). Structure and compressive properties of invar-cenosphere syntactic foams. *Materials, 9*(2), 115.

56. Xue, X. B., Zhao, Y. Y., Kearns, V., & Williams, R. L. (2010). Mechanical and biological properties of titanium syntactic foams. In *TMS 2010 Annual Meeting and Exhibition.* Warrendale.

57. Xue, X., & Zhao, Y. (2011). Ti matrix syntactic foam fabricated by powder metallurgy: Particle breakage and elastic modulus. *JOM, 63*(2), 43–47.

58. Santa Maria, J. A., Schultz, B. F., Ferguson, J. B., & Rohatgi, P. K. (2013). Al–Al2O3 syntactic foams—Part I: Effect of matrix strength and hollow sphere size on the quasi-static properties of Al-A206/Al2O3 syntactic foams. *Materials Science and Engineering: A, 582,* 415–422.

59. Santa Maria, J. A., Schultz, B. F., Ferguson, J. B., Gupta, N., & Rohatgi, P. K. (2014). Effect of hollow sphere size and size distribution on the quasi-static and high strain rate compressive properties of Al-A380–Al2O3 syntactic foams. *Journal of Materials Science, 49*(3), 1267–1278.

60. Goel, M. D., Mondal, D. P., Yadav, M. S., & Gupta, S. K. (2014). Effect of strain rate and relative density on compressive deformation behavior of aluminum cenosphere syntactic foam. *Materials Science and Engineering: A, 590,* 406–415.

61. Cox, J., Luong, D., Shunmugasamy, V., Gupta, N., Strbik, O., & Cho, K. (2014). Dynamic and Thermal properties of aluminum alloy A356/silicon carbide hollow particle syntactic foams. *Metals, 4*(4), 530.

62. Rocha Rivero, G. A., Schultz, B. F., Ferguson, J. B., Gupta, N., & Rohatgi, P. K. (2013). Compressive properties of Al-A206/SiC and Mg-AZ91/SiC syntactic foams. *Journal of Materials Research, 28*(17), 2426–2435.

63. Tao, X. F., & Zhao, Y. Y. (2009). Compressive behavior of Al matrix syntactic foams toughened with Al particles. *Scripta Materialia, 61*(5), 461–464.

64. Zou, L. C., Zhang, Q., Pang, B. J., Wu, G. H., Jiang, L. T., & Su, H. (2013). Dynamic compressive behavior of aluminum matrix syntactic foam and its multilayer structure. *Materials and Design, 45,* 555–560.

65. Luong, D. D., Strbik, O. M., III, Hammond, V. H., Gupta, N., & Cho, K. (2013). Development of high performance lightweight aluminum alloy/SiC hollow sphere syntactic

foams and compressive characterization at quasi-static and high strain rates. *Journal of Alloys and Compounds, 550,* 412–422.

66. Dou, Z. Y., Jiang, L. T., Wu, G. H., Zhang, Q., Xiu, Z. Y., & Chen, G. Q. (2007). High strain rate compression of cenosphere-pure aluminum syntactic foams. *Scripta Materialia, 57*(10), 945–948.

67. Zhang, L. P., & Zhao, Y. Y. (2007). Mechanical response of Al matrix syntactic foams produced by pressure infiltration casting. *Journal of Composite Materials, 41*(17), 2105–2117.

68. Mondal, D. P., Goel, M. D., & Das, S. (2009). Compressive deformation and energy absorption characteristics of closed cell aluminum-fly ash particle composite foam. *Materials Science and Engineering: A, 507*(1–2), 102–109.

69. Rabiei, A., & O'Neill, A. T. (2005). A study on processing of a composite metal foam via casting. *Materials Science and Engineering: A, 404*(1–2), 159–164.

70. Vendra, L., Neville, B., & Rabiei, A. (2009). Fatigue in aluminum–steel and steel–steel composite foams. *Materials Science and Engineering: A, 517*(1–2), 146–153.

71. Neville, B. P., & Rabiei, A. (2008). Composite metal foams processed through powder metallurgy. *Materials and Design, 29*(2), 388–396.

72. Newsome, D., Schultz, B., Ferguson, J., & Rohatgi, P. (2015). Synthesis and quasi-static compressive properties of Mg-AZ91D-Al2O3 syntactic foams. *Materials, 8*(9), 5292.

73. Daoud, A. (2008). Synthesis and characterization of novel ZnAl22 syntactic foam composites via casting. *Materials Science and Engineering: A, 488*(1–2), 281–295.

74. Anantharaman, H., Shunmugasamy, V. C., Strbik, O. M., III, Gupta, N., & Cho, K. (2015). Dynamic properties of silicon carbide hollow particle filled magnesium alloy (AZ91D) matrix syntactic foams. *International Journal of Impact Engineering, 82,* 14–24.

75. Tagliavia, G., Porfiri, M., & Gupta, N. (2011). Analysis of particle-to-particle elastic interactions in syntactic foams. *Mechanics of Materials, 43*(12), 952–968.

76. Bharath Kumar, B. R., Zeltmann, S. E., Doddamani, M., Gupta, N., Uzma, Gurupadu, S., & Sailaja, R. R. N. (2016). Effect of cenosphere surface treatment and blending method on the tensile properties of thermoplastic matrix syntactic foams. *Journal of Applied Polymer Science, 133*(35), n/a–n/a.

77. Tagliavia, G., Porfiri, M., & Gupta, N. (2010). Analysis of hollow inclusion–matrix debonding in particulate composites. *International Journal of Solids and Structures, 47*(16), 2164–2177.

78. Zeltmann, S. E., Prakash, K. A., Doddamani, M., & Gupta, N. (2017). Prediction of modulus at various strain rates from dynamic mechanical analysis data for polymer matrix composites. *Composites Part B: Engineering, 120,* 27–34.

79. Zeltmann, S. E., Bharath Kumar, B. R., Doddamani, M., & Gupta, N. (2016). Prediction of strain rate sensitivity of high density polyethylene using integral transform of dynamic mechanical analysis data. *Polymer, 101,* 1–6.

80. Gupta, N., & Shunmugasamy, V. C. (2011). High strain rate compressive response of syntactic foams: Trends in mechanical properties and failure mechanisms. *Materials Science and Engineering: A, 528*(25–26), 7596–7605.

81. Ahmadi, H., Liaghat, G., Shokrieh, M., Hadavinia, H., Ordys, A., & Aboutorabi, A. (2015). Quasi-static and dynamic compressive properties of ceramic microballoon filled syntactic foam. *Journal of Composite Materials, 49*(10), 1255–1266.

82. Goel, M. D., Peroni, M., Solomos, G., Mondal, D. P., Matsagar, V. A., Gupta, A. K., et al. (2012). Dynamic compression behavior of cenosphere aluminum alloy syntactic foam. *Materials and Design, 42,* 418–423.

83. Karlos, V., & Solomos, G. (2013). *Calculation of blast loads for application to structural components.* Publications Office of the European Union, Luxembourg, p. JRC Technical Reports: EUR 26456 EN.

84. Porfiri, M., & Gupta, N. (2010). A review of research on impulsive loading of marine composites. In I. M. Daniel, E. E. Gdoutos, & Y. D. S. Rajapakse (Eds.), *Major*

accomplishments in composite materials and sandwich structures (pp. 169–194). Springer Netherlands: Dordrecht.

85. Hause, T. (2012). Elastic structural response of anisotropic sandwich plates with a first-order compressible core impacted by a Friedlander-type shock loading. *Composite Structures, 94* (5), 1634–1645.

86. Peroni, L., Scapin, M., Avalle, M., Weise, J., Lehmhus, D., Baumeister, J., et al. (2012). Syntactic iron foams—on deformation mechanisms and strain-rate dependence of compressive properties. *Advanced Engineering Materials, 14*(10), 909–918.

87. 3M. (2017). *3M™ Glass Bubbles S60HS*. Retrieved April 28, 2017, from http://multimedia.3m.com/mws/media/184506O/3mtm-glass-bubbles-s60hs.pdf.

88. Ryan, A. A., David, L. M., & David, J. B. (2006). Numerical simulation of shock wave propagation in spatially-resolved particle systems. *Modelling and Simulation in Materials Science and Engineering, 14*(4), 537.

89. Marsh, S. P. (1980). *LASL shock Hugoniot data* (vol. 5). University of California Press.

90. Christou, G. A., Young, L. R., Goel, R., Vechart, A. P., & Jérusalem, A. (2012). Shock attenuation of PMMA sandwich panels filled with soda-lime glass beads: A fluid-structure interaction continuum model simulation. *International Journal of Impact Engineering, 47,* 48–59.

91. Johnson, G. R., & Cook, W. H. (1985). Fracture characteristics of three metals subjected to various strains, strain rates, temperatures and pressures. *Engineering Fracture Mechanics, 21*(1), 31–48.

92. Caeti, R., Gupta, N., & Porfiri, M. (2009). Processing and compressive response of functionally graded composites. *Materials Letters, 63*(22), 1964–1967.

93. Gupta, N. (2007). A functionally graded syntactic foam material for high energy absorption under compression. *Materials Letters, 61*(4–5), 979–982.

94. Omar, M. Y., Xiang, C., Gupta, N., Strbik, O. M., III, & Cho, K. (2015). Syntactic foam core metal matrix sandwich composite under bending conditions. *Materials and Design, 86,* 536–544.

95. Lamanna, E., Gupta, N., Cappa, P., Strbik, O. M., III, & Cho, K. (2017). Evaluation of the dynamic properties of an aluminum syntactic foam core sandwich. *Journal of Alloys and Compounds, 695,* 2987–2994.

96. Gupta, N., Kishore, & Sankaran, S. (1999). On the characterisation of syntactic foam core sandwich composites for compressive properties. *Journal of Reinforced Plastics and Composites, 18*(14), 1347–1357

97. Abaqus. (2012). *Abaqus Analysis User's Manual (6.12)*.

98. Deshpande, V. S., & Fleck, N. A. (2000). Isotropic constitutive models for metallic foams. *Journal of the Mechanics and Physics of Solids, 48*(6–7), 1253–1283.